

A Mathematical Study of the Differential Effects of Two SERCA Isoforms on Ca^{2+} Oscillations in Pancreatic Islets

Richard Bertram^{a,b,*}, Rudy C. Arceo II^a

^aDepartment of Mathematics, Florida State University, Tallahassee, FL 32306, USA

^bPrograms in Neuroscience and Molecular Biophysics, Florida State University, Tallahassee, FL 32306, USA

Received: 23 July 2007 / Accepted: 19 December 2007 / Published online: 1 February 2008
© Society for Mathematical Biology 2008

Abstract Cytosolic Ca^{2+} dynamics are important in the regulation of insulin secretion from the pancreatic β -cells within islets of Langerhans. These dynamics are sculpted by the endoplasmic reticulum (ER), which takes up Ca^{2+} when cytosolic levels are high and releases it when cytosolic levels are low. Calcium uptake into the ER is through sarcoendoplasmic reticulum Ca^{2+} -ATPases, or SERCA pumps. Two SERCA isoforms are expressed in the β -cell: the high Ca^{2+} affinity SERCA2b pump and the low affinity SERCA3 pump. Recent experiments with islets from SERCA3 knockout mice have shown that the cytosolic Ca^{2+} oscillations from the knockout islets are characteristically different from those of wild type islets. While the wild type islets often exhibit compound Ca^{2+} oscillations, composed of fast oscillations superimposed on much slower oscillations, the knockout islets rarely exhibit compound oscillations, but produce slow (single component) oscillations instead. Using mathematical modeling, we provide an explanation for this difference. We also investigate the effect that SERCA2b inhibition has on the model β -cell. Unlike SERCA3 inhibition, we demonstrate that SERCA2b inhibition has no long-term effect on cytosolic Ca^{2+} oscillations unless a store-operated current is activated.

Keywords Mathematical model · Beta cell · Bursting · Fast-slow analysis

1. Introduction

Insulin secretion from pancreatic islets is pulsatile, reflecting pulsatility in islet intracellular Ca^{2+} levels and the electrical activity of the insulin-secreting β -cells. These oscillations may be fast, with period of less than one minute (Bergsten, 1995; Cook et al., 1981; Henquin, 1988; Santos et al., 1991), or slow with period of 2–7 minutes (Beauvois et al., 2006; Bergsten et al., 1994; Zhang et al., 2003). The slow oscillations in Ca^{2+} levels

*Corresponding author.

E-mail address: Bertram@math.fsu.edu (Richard Bertram).

have period similar to the period of *in vivo* pulsatile insulin measurements (Bergsten and Hellman, 1993; Nunemaker et al., 2005; Pørksen et al., 1995). One type of slow Ca^{2+} oscillation is characterized by plateaus of elevated Ca^{2+} and is due to long bursts of action potentials, called slow bursting (Zhang et al., 2003). The other type is characterized by slow plateaus with fast oscillations superimposed (Zhang et al., 2003). This is due to periodic episodes of fast bursts, and is called compound bursting (Bertram et al., 2004; Cook, 1983; Henquin et al., 1982). Thus, compound bursting consists of “inner oscillations” which are the fast bursts, and “outer oscillations” that group the fast bursts into periodic clusters.

The Ca^{2+} dynamics of β -cells are influenced by Ca^{2+} influx through L-type Ca^{2+} channels and efflux through plasma membrane pumps. In addition, the endoplasmic reticulum (ER) takes up Ca^{2+} from the cytosol when the cytoplasmic Ca^{2+} levels are high (such as when the cell is depolarized) and releases it back into the cytosol when the cytoplasmic Ca^{2+} levels are low (when the cell is hyperpolarized), and thus has a large influence on the cytosolic Ca^{2+} dynamics (Arredouani et al., 2002b; Bertram and Sherman, 2004b). Calcium is pumped into the ER through sarco-endoplasmic reticulum Ca^{2+} -ATPase (SERCA) pumps. In β -cells, two SERCA genes are expressed, SERCA2b and SERCA3 (Arredouani et al., 2002a; Váradi et al., 1996). The SERCA2b pump has high affinity for Ca^{2+} , while SERCA3 has a low affinity (Arredouani et al., 2002a).

Recent experiments with SERCA3 knockout (SERCA3^{-/-}) mice have characterized the contribution of SERCA3 to the Ca^{2+} dynamics of mouse islets (Arredouani et al., 2002a; Beauvois et al., 2006). Here it was shown that the amplitude of the Ca^{2+} responses to a train of long depolarizations was greater in SERCA3^{-/-} islets, and that Ca^{2+} did not accumulate from one pulse to the next. In one report, it was shown that while islets from wild type mice exhibited either slow or compound bursting oscillations, islets from SERCA3^{-/-} mice exhibited only slow oscillations (Beauvois et al., 2006).

In this article, we use mathematical and computational analysis to distinguish the influence of the two SERCA isoforms on the cytosolic and ER calcium dynamics in a model β -cell. We first demonstrate that the model β -cell accounts for the experimental observation that islets from SERCA3^{-/-} mice exhibit slow, but not compound, bursting. We also predict that inhibition of the SERCA2b isoform rather than the SERCA3 isoform would have only transient effects on the cytosolic Ca^{2+} dynamics; the long-term behavior would be the same as before the SERCA2b inhibition unless a store-operated current (SOC) is activated. Thus, if a long-term effect is observed when the SERCA2b pump is inhibited, then this indicates that SOC is activated. To our knowledge, such experiments have not been performed. Whichever isoform is inhibited, the model predicts that there would be a long-term decrease in the ER Ca^{2+} concentration. Indeed, the primary role of SERCA2b may be to maintain the basal ER Ca^{2+} at an elevated level relative to the cytosol.

The β -cell model that we employ, the Dual Oscillator Model, has compartments for electrical activity, Ca^{2+} dynamics, glycolysis, and mitochondrial metabolism (Bertram et al., 2007a). To analyze the differential effects of the two SERCA isoforms, we begin by studying the Ca^{2+} compartment of the model separately from the electrical, glycolytic, and metabolic compartments. Here we simulate the Ca^{2+} response to a train of long membrane depolarizations, similar to what was done experimentally (Arredouani et al., 2002a). We derive formulas for the nadir, plateau, and amplitude of the cytosolic Ca^{2+} response, as well as the temporal mean of the ER Ca^{2+} concentration. Using these formulas, we

show that changes in the SERCA2b pump rate have no long-term effect on the cytosolic Ca^{2+} during the pulse train, but a reduction in the SERCA3 pump rate increases the amplitude of the cytosolic Ca^{2+} response. This demonstrates that the effects on cytosolic Ca^{2+} of the general SERCA pump blocker thapsigargin reported in Arredouani et al. (2002b) and simulated in Bertram and Sherman (2004b) were due to the inhibitory action on SERCA3 pumps. Although SERCA2b pumps would also be inhibited by thapsigargin, this would have no long-term effect on cytosolic Ca^{2+} .

In the final stage of the analysis, we combine the calcium and electrical compartments of the model to demonstrate that reducing the SERCA3 pump rate converts fast bursting (i.e., the inner bursting of a compound burst) to very fast bursting or continuous spiking. This explains why compound Ca^{2+} oscillations are not observed in islets from SERCA3^{-/-} mice; the fast inner bursting is replaced by very fast bursting or continuous spiking, and the outer oscillations remain largely unchanged. In contrast, we show that inhibiting SERCA2b rather than SERCA3 has no long-term effect on the Ca^{2+} profile, unless the ER Ca^{2+} falls to a sufficiently low value that a store-operated current is activated. Such a current has been reported in β -cells (Mears and Zimlik, 2004; Roe et al., 1998), although the ER Ca^{2+} threshold for activation of the current is not known.

2. Mathematical model

The β -cell model is described in detail in Bertram et al. (2007a). It has compartments for electrical activity, cytosolic and ER calcium dynamics, glycolysis, and mitochondrial metabolism. Fig. 1 illustrates the model compartments and the variables in each compartment. Each variable is described by an ordinary differential equation, and many of these equations are coupled, as indicated with arrows in the figure. All expressions and parameter values for the model are given and described in detail in Bertram et al. (2007a), and computer programs are available for free download at www.math.fsu.edu/~bertram/software.

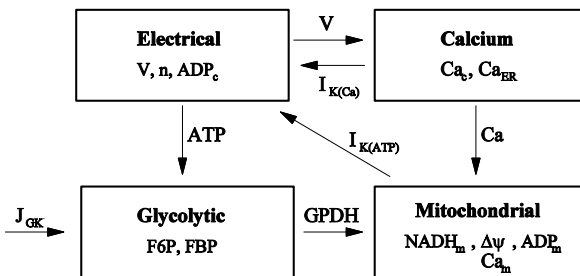


Fig. 1 The four model compartments and coupling pathways among the components. Depolarization of the plasma membrane leads to Ca^{2+} entry and an increase in Ca_c . This in turn activates the $\text{K}(\text{Ca})$ current, leading to hyperpolarization of the membrane. The membrane is also hyperpolarized by the ATP-dependent K^+ current. Cytosolic ATP inhibits the key glycolytic enzyme PFK, and (possibly oscillatory) output from the glycolytic subsystem serves as input to the mitochondrial subsystem. Calcium from the cytosol is also a source of input to the mitochondria.

We begin with the glycolytic compartment. It has been shown that glycolytic activity can be oscillatory in muscle extracts (Tornheim and Lowenstein, 1975). The critical enzyme for these oscillations is phosphofructokinase (PFK), which phosphorylates the substrate fructose 6-phosphate (F6P) to form fructose 1, 6-bisphosphate (FBP) (Tornheim and Lowenstein, 1976). Positive feedback of FBP onto PFK can lead to oscillations of the PFK reaction rate with a period of several minutes in muscle extracts (Smolen, 1995; Tornheim, 1979; Tornheim and Lowenstein, 1974). The muscle type of PFK (PFK-M) is the most active PFK isoform in β -cells (Yaney et al., 1995), and there is direct (Tornheim, 1997) and indirect (Bertram et al., 2004; Dahlgren et al., 2005) evidence for glycolytic oscillations in β -cells. In the Dual Oscillator Model, glycolytic oscillations provide the slow component of the oscillations in islet activity. Thus, in compound bursting, the slow outer oscillations are due to oscillatory glycolysis. The glycolytic model that we use, which is described in detail in Bertram et al. (2004), contains equations for the dynamics of the key enzyme PFK-M and has variables for the PFK substrate and product. Differential equations for these variables are:

$$\frac{dG6P}{dt} = J_{GK} - J_{PFK}, \quad (1)$$

$$\frac{dFBP}{dt} = J_{PFK} - \frac{1}{2} J_{GPDH}. \quad (2)$$

Here G6P is the glucose 6-phosphate concentration, which is assumed to be in rapid equilibrium with F6P ($F6P = 0.3 G6P$). Also, J_{GK} is the glucokinase reaction rate, J_{PFK} is the PFK reaction rate, and J_{GPDH} is the glycerol phosphate dehydrogenase (GPDH) reaction rate. The glucokinase rate serves as input to the system, since it reflects the glucose concentration. The GPDH rate serves as the output of the glycolytic subsystem, since glycolytic reactions downstream of GPDH do not contribute to the generation of glycolytic oscillations and are not included in the model.

The mitochondrial compartment describes the reactions that take place during oxidative phosphorylation. It includes an expression for Ca^{2+} -dependent dehydrogenases of the citric acid cycle, yielding NADH. The NADH supplies electrons for the electron transport chain, which produces a membrane potential across the mitochondrial inner membrane, $\Delta\psi$. The flux of protons down the electrical gradient through the F_1F_0 -ATP synthase converts ADP to ATP. Finally, Ca^{2+} enters the mitochondria through Ca^{2+} uniporters and is transported out through Na^+/Ca^{2+} exchangers. The mitochondrial compartment has variables for the NADH, ADP, and mitochondrial Ca^{2+} concentrations, and for $\Delta\psi$. The ATP concentration is calculated from the ADP concentration by assuming that the sum of the two is conserved. Differential equations for the mitochondrial variables are:

$$\frac{dNADH_m}{dt} = \gamma(J_{DH} - J_O), \quad (3)$$

$$\frac{d\Delta\psi}{dt} = (J_{H,res} - J_{H,atp} - J_{ANT} - J_{H,leak} - J_{NaCa} - 2J_{uni})/C_m, \quad (4)$$

$$\frac{dCa_m}{dt} = f_m(J_{uni} - J_{NaCa}), \quad (5)$$

$$\frac{dADP_m}{dt} = \gamma(J_{ANT} - J_{F1F0}). \quad (6)$$

Here J_{DH} is the reaction rate of the citric acid dehydrogenases, J_O is oxygen consumption, $J_{H,res}$ is the respiration-driven proton efflux, $J_{H,atp}$ is proton influx through the ATP synthase, J_{ANT} is flux through the adenine nucleotide translocator, $J_{H,leak}$ is proton leak across the mitochondrial inner membrane, J_{NaCa} is Ca^{2+} efflux through the electrogenic Na^+/Ca^{2+} exchanger, and J_{uni} is Ca^{2+} influx through uniporters.

The electrical compartment describes the plasma membrane potential (V) and includes a variable (n) for the fraction of activated delayed rectifier K^+ channels. The membrane potential is determined by the flux of ions through several types of ion channels:

$$\frac{dV}{dt} = -(I_K + I_{Ca} + I_{K(Ca)} + I_{K(ATP)} + I_{SOC})/C_{pm}, \quad (7)$$

$$\frac{dn}{dt} = \frac{n_{\infty}(V) - n}{\tau_n}. \quad (8)$$

Here I_K is the delayed rectifier current, I_{Ca} is an L-type Ca^{2+} current, $I_{K(Ca)}$ is a Ca^{2+} -activated K^+ current, and $I_{K(ATP)}$ is an ATP-sensitive K^+ current. C_{pm} denotes the membrane capacitance. The activation variable n satisfies first order kinetics, and has equilibrium function $n_{\infty}(V)$. Finally, we add a store-operated current (I_{SOC}) to the model of Bertram et al. (2007a). This current activates when the ER Ca^{2+} concentration falls below a threshold, and we model it as in Bertram et al. (1995b):

$$I_{SOC} = \bar{g}_{SOC} x_{\infty}(Ca_{er})(V - V_{SOC}), \quad (9)$$

where $\bar{g}_{SOC} = 50$ pS is the maximum conductance, $V_{SOC} = 0$ mV is the reversal potential, and

$$x_{\infty}(Ca_{er}) = \frac{1}{1 + \exp(Ca_{er} - \overline{Ca_{er}})} \quad (10)$$

is the sigmoidal activation function. We use an activation threshold of $\overline{Ca_{er}} = 70$ μ M.

There is also an equation for the cytosolic ADP concentration:

$$\frac{dADP_c}{dt} = J_{hyd} - \kappa J_{ANT}. \quad (11)$$

Here J_{hyd} is the hydrolysis rate of ATP to ADP. The cytosolic ATP concentration is derived from the ADP concentration by assuming that the sum of the two is conserved.

The cytosolic Ca^{2+} concentration is determined by Ca^{2+} flux across the plasma membrane (J_{mem}), the ER membrane (J_{ER}), and the mitochondrial membrane (J_m). It is described by:

$$\frac{dCa_c}{dt} = f_c(J_{mem} + J_{er} + \kappa J_m). \quad (12)$$

Here f_c is the fraction of Ca^{2+} that is unbound by buffers and κ is the mitochondria-to-cytosol volume ratio. The flux across the plasma membrane is

$$J_{mem} = -(\alpha I_{Ca} + k_{PMCA}(Ca_c - Ca_{bas})), \quad (13)$$

where α converts current to flux, k_{PMCA} is the plasma membrane pump rate, and Ca_{bas} is a constant basal Ca^{2+} parameter. I_{Ca} is the Ca^{2+} current, $I_{\text{Ca}} = \bar{g}_{\text{Ca}} m_{\infty}(V)(V - V_{\text{Ca}})$, where $m_{\infty}(V)$ is the equilibrium fraction of activated Ca^{2+} channels. Flux out of the ER is assumed to occur only through passive leakage (IP₃ receptors are not activated),

$$J_{\text{leak}} = p_{\text{leak}}(\text{Ca}_{\text{er}} - \text{Ca}_{\text{c}}). \quad (14)$$

Flux into the ER from the cytosol is through SERCA2b and SERCA3 pumps, $J_{\text{SERCA}} = J_{2b} + J_3$. Since SERCA2b has a high affinity for Ca^{2+} , we assume that the pumps are saturated at physiological Ca^{2+} levels, so that the SERCA2b pump rate is independent of the Ca^{2+} concentration ($J_{2b} = k_{2b}$, where k_{2b} is a parameter). The SERCA3 pump rate has low affinity, and we assume a linear dependence on Ca^{2+} , $J_3 = k_3 \text{Ca}_{\text{c}}$. Thus,

$$J_{\text{SERCA}} = k_{2b} + k_3 \text{Ca}_{\text{c}}, \quad (15)$$

and

$$J_{\text{er}} = J_{\text{leak}} - J_{\text{SERCA}}. \quad (16)$$

Finally, the differential equation for the ER Ca^{2+} concentration is:

$$\frac{d\text{Ca}_{\text{er}}}{dt} = -f_{\text{er}} \nu J_{\text{er}}, \quad (17)$$

where f_{er} is the fraction of free Ca^{2+} in the ER, and $\nu = V_{\text{c}}/V_{\text{er}}$ is the cytosol-to-ER volume ratio.

The differential equations are solved numerically using the XPPAUT software package (Ermentrout, 2002). The CVODE integration method is used, with tolerances of 10^{-9} .

3. SERCA3 inhibition converts compound bursting to slow bursting

In the mathematical model, the combination of slow glycolytic oscillations and fast bursting driven by Ca^{2+} feedback onto K(Ca) ion channels produces compound bursting (Fig. 2). The several-minute period of this bursting is set by the period of the glycolytic oscillations. These oscillations are reflected in oscillatory levels of the glycolytic product FBP (Fig. 2C). During the phase of the oscillation when glycolytic output is high the mitochondrial ATP production is also high. This inhibits K(ATP) channels (Ashcroft et al., 1984) and depolarizes the model cell. The subsequent Ca^{2+} -driven action potentials cause Ca^{2+} to accumulate in the cytosol and ER, and the elevated level of cytosolic Ca^{2+} (Fig. 2B) activates K(Ca) channels. The resulting hyperpolarizing current terminates the fast burst of action potentials. The cytosolic Ca^{2+} level then declines, and when it reaches a sufficiently low level a new fast burst is initiated. Thus, the inner fast bursts are due to the dynamics of the electrical and Ca^{2+} subsystems, while the outer slow oscillation that clusters the bursts together is due to glycolytic oscillations acting through the ATP-producing mitochondrial component of the model.

During a burst episode (Fig. 3A) there is a net influx of Ca^{2+} into the ER, so the ER Ca^{2+} concentration increases. The series of inner bursts that occur during a compound

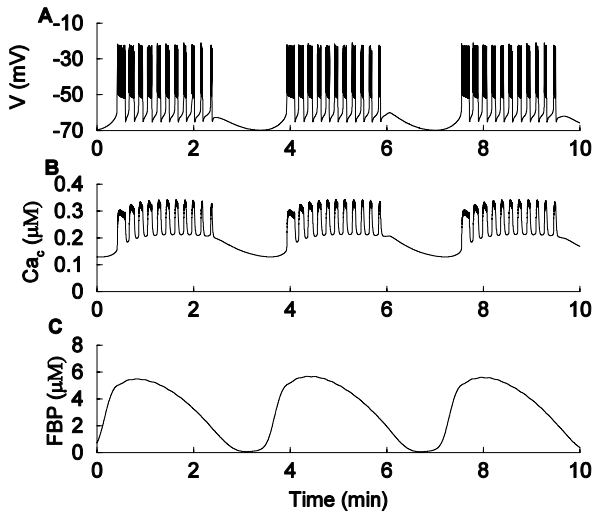


Fig. 2 (A) Compound bursting produced with $J_{GK} = 0.4 \mu\text{Mms}^{-1}$. (B) Ca^{2+} concentration is elevated during each episode of compound bursting. (C) Slow oscillations of the glycolytic product FBP provide the metabolic input to mitochondria, which in turn produce ATP that is responsible for clustering fast bursts into episodes.

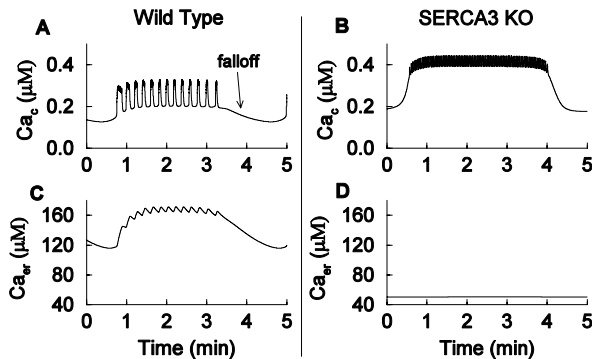


Fig. 3 Compound bursting is converted to slow bursting when the SERCA3 pump is “knocked out” ($k_3 = 0$). (A) A compound bursting oscillation with a series of fast inner bursts. There is a slow falloff of Ca^{2+} at the end of a burst episode. (B) A slow bursting oscillation is produced when SERCA3 is knocked out. The slow Ca^{2+} falloff is no longer present. (C) In the “wild type” cell (SERCA3 not inhibited), the ER Ca^{2+} concentration exhibits a plateau when glycolytic output is high, with superimposed small fluctuations reflecting the fast inner bursting of the compound burst. (D) In the SERCA3 KO Ca_{er} is at a constant low level.

burst results in small fluctuations of Ca_{er} , which are superimposed on a larger plateau (Fig. 3C). At the end of a burst episode Ca^{2+} slowly drains from the ER into the cytosol. Thus, even though there is no influx into the cytosol through ion channels during the inter-

episode phase, there is influx from the ER. For this reason, the decline of Ca_c during the inter-episode phase is slow, i.e., there is a slow falloff of Ca_c (Fig. 3A).

When the SERCA3 pumps are inhibited by setting $k_3 = 0$ there is a dramatic change in the Ca^{2+} dynamics (Fig. 3B). The slow envelope of the oscillation is relatively unchanged, but now the fast inner bursting is converted to tonic spiking. Thus, the compound bursting is converted to slow bursting. This agrees with experimental findings of Beauvois et al. that slow, but not compound, Ca^{2+} oscillations were observed in islets from SERCA3^{-/-} mice, while both slow and compound oscillations were observed in islets from wild type mice (Beauvois et al., 2006). In our model, Ca_{er} declines to a relatively low level in the simulated SERCA3 knockout and no longer exhibits plateau or low-amplitude oscillations (Fig. 3D). This is as expected, since one of the SERCA pumps has been inhibited and the only remaining pump, SERCA2b, is independent of Ca^{2+} . (SERCA2b has high Ca^{2+} affinity, and we assume that it is saturated at basal Ca^{2+} levels.) Because the ER no longer contributes Ca^{2+} to the cytosol during the inter-episode phase, Ca_c no longer exhibits a slow falloff during this phase.

Other experimental studies have examined cytosolic Ca^{2+} measurements in stimulatory glucose concentrations after application of the SERCA pump blocker thapsigargin (Tg). This blocker affects both the SERCA3 and SERCA2b isoforms. It was found that slow, but not compound, Ca^{2+} oscillations were produced, and that the slow cytosolic Ca^{2+} falloff observed in control islets was not observed when SERCA pumps were blocked with Tg (Gilon et al., 1999; Liu et al., 1995, 1998; Miura et al., 1997). The model produces similar behavior when SERCA3 pumps (Fig. 3) or both SERCA3 and SERCA2b pumps (not shown) are inhibited.

Two factors are involved in the change of Ca^{2+} dynamics that occurs when the SERCA3 pumps are inhibited. One factor is that the ER is no longer taking up Ca^{2+} when the model cell is electrically active and giving it back when the cell is silent. That is, the Ca^{2+} filtering that normally takes place by the ER (Bertram and Sherman, 2004b) has been inhibited. This factor is examined later in the article. The other factor is that Ca_{er} has declined to a level sufficiently low to activate the store-operated current, I_{SOC} . In the model, activation of this current begins when Ca_{er} falls below 70 μ M, as when SERCA3 is inhibited in Fig. 3D. By increasing the pumping rate of SERCA2b so that Ca_{er} rises above 70 μ M, it may be possible to compensate for the effects of SERCA3 knockout. This possibility is examined in Fig. 4. In this simulation, the SERCA2b pump rate is increased (k_{2b} increased from 0.01 μ Mms⁻¹ to 0.03 μ Mms⁻¹) at the same time that the SERCA3 pump rate is set to 0. The increased SERCA2b pumping does increase Ca_{er} to a much higher level (Fig. 4D) than in Fig. 3D, so that I_{SOC} is no longer activated. However, the compound bursting is still converted to a pattern that is similar to slow bursting (Fig. 4B). This pattern consists of episodes of fast bursts, but the fast bursts are so fast (period \approx 2 sec) that they would likely be classified as tonic spiking, particularly if the temporal resolution of the Ca^{2+} imaging is not high enough to resolve the very fast bursts. Thus, in this example, increasing the SERCA2b pump rate does not compensate for the effects on the cytosolic Ca^{2+} pattern of inhibiting the SERCA3 pumps. We show later (Sections 7 and 8) that this is a general result, i.e., it is not possible for an increase in the SERCA2b pump rate to compensate for inhibition of SERCA3 pumps.

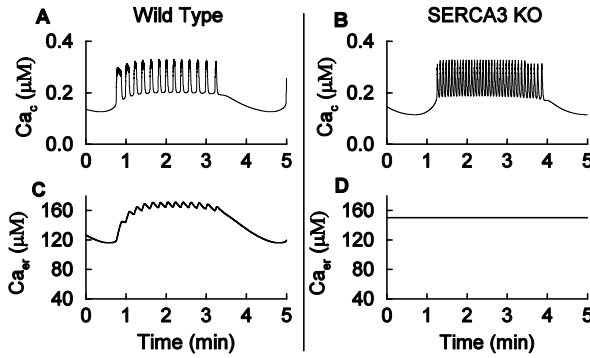


Fig. 4 Increasing SERCA2b pumping cannot compensate for loss of SERCA3 pumping. In the SERCA3 knockout ($k_3 = 0$), the SERCA2b pump rate k_2 is increased from $0.01 \mu\text{Mms}^{-1}$ to $0.03 \mu\text{Mms}^{-1}$. This increases Ca_{er} so that I_{SOC} is not activated (D), but the compound bursting oscillation (A) is still converted to a pattern resembling slow bursting (B) when SERCA3 pumping is eliminated.

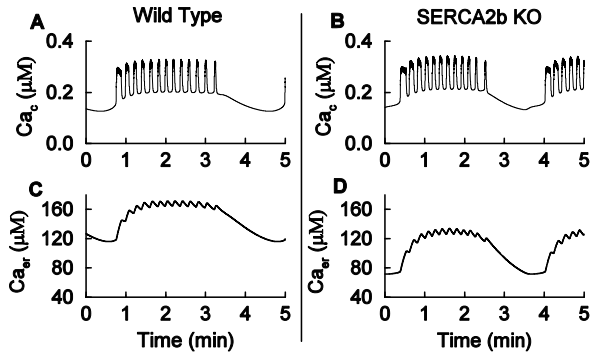


Fig. 5 Knocking out SERCA2b ($k_{2b} = 0$) has little effect on the compound bursting time course (B), even though the ER Ca^{2+} concentration is reduced by a third of its original value (D).

4. SERCA2b removal has little effect on the cytosolic Ca^{2+} time course

We next tested to see what effect removal of SERCA2b pumps would have on the compound bursting oscillation. Fig. 5 shows that eliminating SERCA2b pumping ($k_{2b} = 0$) has only a minor effect on the cytosolic Ca^{2+} time course (SERCA3 has not been inhibited). This is in spite of the fact that the ER Ca^{2+} concentration is reduced by a third (Fig. 5D). What little effect there is on the cytosolic Ca^{2+} time course is due to activation of the SOC current that results from the reduction in the mean ER Ca^{2+} concentration. If the SOC conductance is set to 0, then eliminating SERCA2b has no effect at all on the cytosolic Ca^{2+} time course. The reason for this lack of effect of SERCA2b inhibition is not obvious, but will be clarified later.

5. Voltage clamp protocol simplifies analysis of the model

As a first step in understanding the differential effects of the two SERCA knockouts, we focus on the Ca^{2+} subsystem. To bypass the dynamics of the electrical subsystem, a voltage clamp protocol is used that captures the pacemaker dynamics of fast bursting (Bertram and Sherman, 2004b). In this protocol, the voltage is originally clamped at -70 mV. It is then increased to -60 mV, representative of a silent phase of a burst. To simulate a burst active phase the voltage is increased to -40 mV for 8 sec. This is followed by a return to -60 mV for 16 sec (silent phase), and another increase to -40 mV (active phase). This continues in a periodic fashion (Fig. 6A). The duration of the depolarizations and repolarizations are similar to the durations of active and silent phases during fast bursting.

To simplify the analysis, and focus on the cytosol-ER interactions, the contribution of the mitochondrial Ca^{2+} store is excluded from the cytosolic Ca^{2+} equation. We also set $C_{\text{bas}} = 0$. The Ca^{2+} equation is then

$$\frac{dC_{\text{ac}}}{dt} = f_c(J_{\text{mem}} + J_{\text{er}}). \quad (18)$$

The cytosolic Ca^{2+} response to the voltage clamp protocol is shown in Fig. 6B (black curve). Notice that C_{ac} rises quickly during the depolarization and falls quickly during the repolarization. Thus, it adjusts rapidly to changes in V . We take advantage of this by using a rapid equilibrium approximation. That is, we assume that C_{ac} adjusts instantaneously to changes in V , and set the derivative in Eq. (18) to 0. We then solve the resulting algebraic equation for C_{aEQ} , the rapid-equilibrium cytosolic Ca^{2+} concentration:

$$C_{\text{aEQ}} = \frac{J_{\text{in}} - k_{2b} + p_{\text{leak}}C_{\text{aer}}}{k_{\text{pmca}} + k_3 + p_{\text{leak}}}, \quad (19)$$

where $J_{\text{in}} = -\alpha I_{\text{Ca}}$ is the Ca^{2+} influx through plasma membrane Ca^{2+} channels. The time course of C_{aEQ} during the voltage clamp protocol is shown in Fig. 6B (red curve). The dynamics of C_{aEQ} are quite similar to those of C_{ac} , and one differential equation is removed when C_{aEQ} is used in the model rather than C_{ac} .

The rapid-equilibrium cytosolic Ca^{2+} concentration can be incorporated into the differential equation for the ER Ca^{2+} concentration (Eq. (17)) by replacing C_{ac} with C_{aEQ} and using Eq. (19), yielding

$$\frac{dC_{\text{aer}}}{dt} = f_{\text{er}}v[\Omega J_{\text{in}} + (1 - \Omega)(k_{2b} - p_{\text{leak}}C_{\text{aer}})], \quad (20)$$

where

$$\Omega = \frac{k_3 + p_{\text{leak}}}{k_3 + k_{\text{pmca}} + p_{\text{leak}}}. \quad (21)$$

Notice that $0 < \Omega < 1$, so $(1 - \Omega) > 0$.

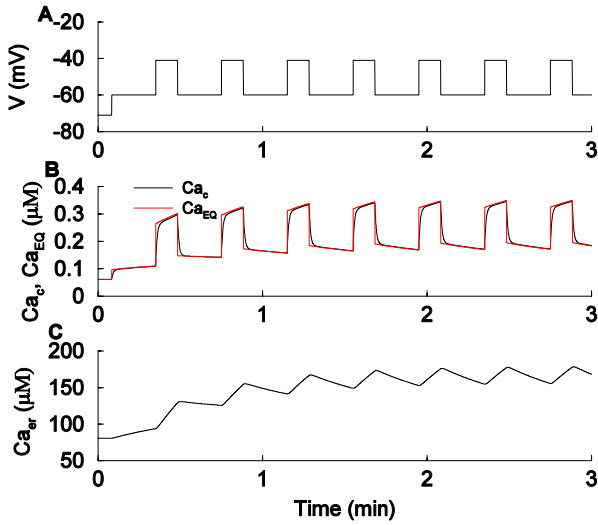


Fig. 6 Analysis of the Ca²⁺ subsystem. (A) Voltage clamp protocol, with durations and voltage values based on a fast bursting pattern (without spikes). (B) Cytosolic Ca²⁺ concentration (black) and the rapid equilibrium approximation (red) during the pulse protocol. The difference between the two is small. (C) The ER Ca²⁺ concentration during the pulse protocol. (Color figure online.)

During the voltage pulse train Ca_{er} rises with two temporal components. There is a fast component, reflecting each voltage depolarization. There is also a slow component, reflecting the cumulative effect of the series of depolarizations. One can remove the fast component by averaging over a single period of the voltage pulse train (i.e., averaged over 24 sec). Let ⟨Ca_{er}⟩ denote Ca_{er} (Eq. (20)) averaged over one period. Then

$$\frac{d\langle\text{Ca}_{er}\rangle}{dt} = f_{er}v[\Omega\langle J_{in}\rangle + (1 - \Omega)(k_{2b} - p_{leak}\langle\text{Ca}_{er}\rangle)]. \tag{22}$$

Here ⟨J_{in}⟩ is the influx of Ca²⁺ over one period, divided by the period. During the depolarized phase (when V = -40 mV) the Ca²⁺ influx rate is J_{in,dep} = 0.0461 μMms⁻¹. During the repolarized phase (when V = -60 mV), the influx rate is J_{in,rep} = 0.0131 μMms⁻¹. The durations of the two phases are T_{dep} = 8 sec and T_{rep} = 16 sec, respectively. Then

$$\langle J_{in}\rangle = \frac{J_{in,dep}T_{dep} + J_{in,rep}T_{rep}}{T_{dep} + T_{rep}} \approx 0.0241 \mu\text{Mms}^{-1}. \tag{23}$$

This mean Ca²⁺ influx can be used in Eq. (22) and the linear differential equation solved, yielding the expression

$$\langle\text{Ca}_{er}\rangle = \lambda_1 e^{\lambda_2 t} - \frac{\lambda_3}{\lambda_2}, \tag{24}$$

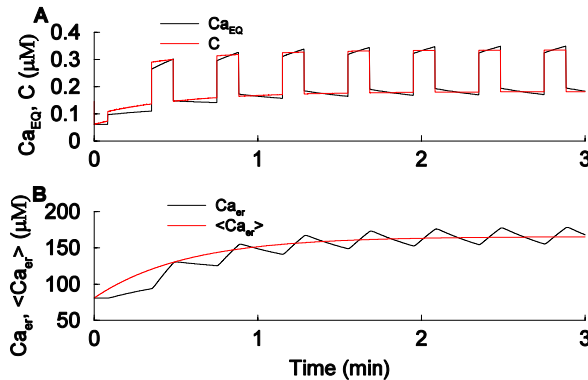


Fig. 7 Comparison of time courses when Ca_{er} or the time averaged Ca_{er} , $\langle Ca_{er} \rangle$ are used to compute the cytosolic Ca^{2+} time course. (A) Cytosolic Ca^{2+} concentrations computed in two ways (Eqs. (17) and (26)). (B) The ER Ca^{2+} concentration (Eq. (18)) and its time average (Eq. (22)). (Color figure online.)

where

$$\lambda_1 = \frac{\lambda_3}{\lambda_2} + \langle Ca_{er} \rangle_0, \quad (25)$$

$$\lambda_2 = -f_{er} \nu (1 - \Omega) p_{leak}, \quad (26)$$

$$\lambda_3 = f_{er} \nu [\Omega \langle J_{in} \rangle + (1 - \Omega) k_{2b}], \quad (27)$$

where $\langle Ca_{er} \rangle_0$ is the initial value of Ca_{er} .

The time-dependent average Ca_{er} , $\langle Ca_{er} \rangle$, can then be inserted into Eq. (19) in place of Ca_{er} , to give an expression for the rapid-equilibrium cytosolic Ca^{2+} concentration with the fast component of the ER Ca^{2+} fluctuations averaged out. That is, this new variable C responds to the slow rise in Ca_{er} that occurs during the train of depolarizations, but not the faster fluctuations of Ca_{er} that occur with each depolarization. The dynamics of C are described by

$$C = \frac{J_{in} - k_{2b} + p_{leak} \langle Ca_{er} \rangle}{k_{pmca} + k_3 + p_{leak}}. \quad (28)$$

Equations (24) and (28) provide a description of the time-dependent changes in Ca^{2+} that consists solely of algebraic equations.

Fig. 7 compares C (Eq. (28)) with Ca_{EQ} (Eq. (19)) during the voltage pulse train. The two are very similar, except that Ca_{EQ} rises a bit more during the depolarized phase and declines a bit more during the repolarized phase. These small rises and falls reflect the small fluctuations in Ca_{er} (computed with Eq. (20)), which are not present in $\langle Ca_{er} \rangle$ (computed with Eq. (24)).

6. Calculation of plateaus, nadirs, and amplitudes of the Ca^{2+} response

With Eq. (28), it is possible to track the values of the cytosolic Ca^{2+} plateaus (during voltage depolarization) and nadirs (during repolarization) over time during the pulse train.

For the plateaus, $J_{in,dep}$ is used rather than J_{in} in Eq. (28), while $J_{in,rep}$ is used for the nadirs. That is,

$$C^{plateau} = \frac{J_{in,dep} - k_{2b} + p_{leak} \langle Ca_{er} \rangle}{k_{pmca} + k_3 + p_{leak}}, \quad (29)$$

$$C^{nadir} = \frac{J_{in,rep} - k_{2b} + p_{leak} \langle Ca_{er} \rangle}{k_{pmca} + k_3 + p_{leak}}. \quad (30)$$

The amplitude of a cytosolic Ca^{2+} response is then

$$C^{amp} = C^{plateau} - C^{nadir} = \frac{J_{in,dep} - J_{in,rep}}{k_{pmca} + k_3 + p_{leak}}. \quad (31)$$

Three things can be deduced from Eq. (31):

- The amplitude of the cytosolic Ca^{2+} response is independent of the ER Ca^{2+} concentration.
- The amplitude is independent of the SERCA2b pump rate (k_{2b}).
- The amplitude decreases when the plasma membrane pump rate (k_{pmca}), SERCA3 pump rate (k_3), or leak rate out of the ER (p_{leak}) are increased.

Thus, the experimental observation that the Ca^{2+} response amplitude to a voltage clamp depolarization is larger in the presence of the SERCA pump blocker thapsigargin (Arredouani et al., 2002b; Gilon et al., 1999) is consistent with Eq. (31) (C^{amp} is larger when k_3 is set to 0).

While it is clear from Eq. (31) that the amplitude of the Ca^{2+} response is independent of k_{2b} , it can also be shown that the long-term or asymptotic values of the plateau and nadir are independent of k_{2b} . That is, the asymptotic value of C is independent of k_{2b} . By “asymptotic value” we mean the value of C after many voltage pulses, once $\langle Ca_{er} \rangle$ has reached its equilibrium value. From Eq. (24), the equilibrium value of $\langle Ca_{er} \rangle$ is

$$\langle Ca_{er} \rangle_{\infty} = -\frac{\lambda_3}{\lambda_2} = \frac{f_{er}\nu[\Omega \langle J_{in} \rangle + (1 - \Omega)k_{2b}]}{f_{er}\nu(1 - \Omega)p_{leak}} = \frac{\Omega \langle J_{in} \rangle}{(1 - \Omega)p_{leak}} + \frac{k_{2b}}{p_{leak}}. \quad (32)$$

The asymptotic value of C is obtained by inserting Eq. (32) into Eq. (28) in place of $\langle Ca_{er} \rangle$,

$$C_{\infty} = \frac{J_{in} - k_{2b} + p_{leak} \langle Ca_{er} \rangle_{\infty}}{k_{pmca} + k_3 + p_{leak}} = \frac{(1 - \Omega)J_{in} + \Omega \langle J_{in} \rangle}{(1 - \Omega)(k_{pmca} + k_3 + p_{leak})}, \quad (33)$$

which is independent of k_{2b} . Thus, the asymptotic values of the plateaus and nadirs of C are independent of k_{2b} . They do, however, depend on the SERCA3 pump rate.

7. SERCA2b inhibition has no effect on fast bursting

We now take the next step in the analysis of how the two SERCA isoforms affect compound bursting. Since compound bursting is composed of episodes of fast bursts, and since it was the fast component of bursting that was affected by inhibition of SERCA3 (Fig. 4),

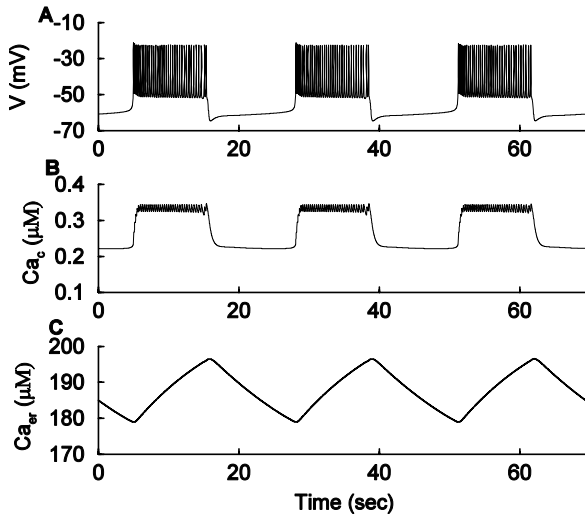


Fig. 8 (A) Fast bursting produced by the electrical/calcium compartments of the model with $g_{K(ATP)} = 170$ pS. (B) Cytosolic Ca^{2+} concentration rises relatively quickly to a plateau during the active phase and falls quickly to a nadir during the silent phase. (C) The ER Ca^{2+} concentration changes on a slower time scale, and the rate of these slow changes sets the period of the bursting oscillation.

we focus on fast bursting. Fast bursting involves the electrical and calcium compartments of the model, with voltage now driven by ionic fluxes rather than voltage clamp as above. To isolate the electrical/calcium compartments from the glycolytic/mitochondrial compartments we set the conductance of the K(ATP) current to a constant value, $g_{K(ATP)} = 170$ pS.

Fig. 8A shows the fast bursting that results when the K(ATP) conductance is clamped. The bursts are produced by slow activity-dependent changes in Ca_c and Ca_{er} . During the active phase of the burst Ca_c rises and reaches a plateau (Fig. 8B). Meanwhile, Ca_{er} rises more slowly (Fig. 8C), and as it rises contributes an ever greater amount of Ca^{2+} to the cytosol. This results in a rise in the mean level of Ca_c . The cytosolic Ca^{2+} has a hyperpolarizing effect on the cell through activation of K(Ca) channels, and the slow rise in the mean Ca_c (and thus K(Ca) conductance) is eventually sufficient to keep the cell below spike threshold, ending the active phase of the burst. During the silent phase Ca_c and Ca_{er} both decline, so that the K(Ca) conductance declines to a level sufficiently small so that spiking is restarted.

To analyze this bursting, we use the standard approach (see Bertram and Sherman, 2004a) of treating the slow variables (Ca_c and Ca_{er}) as constants and then performing a bifurcation analysis on the fast subsystem (V and n). When store operated current is not activated (the case we consider here), Ca_{er} does not enter into the fast subsystem. However, Ca_c is an important parameter of this subsystem. In Fig. 9, we show a bifurcation diagram of the fast subsystem (the “slow manifold”), with Ca_c treated as the bifurcation parameter. The curve marked SS is a branch of stable steady states, while the curves marked US are branches of unstable steady states. The curve marked SP is a branch of stable periodic spiking solutions. Both the maximum (top thick curve) and minimum (bot-

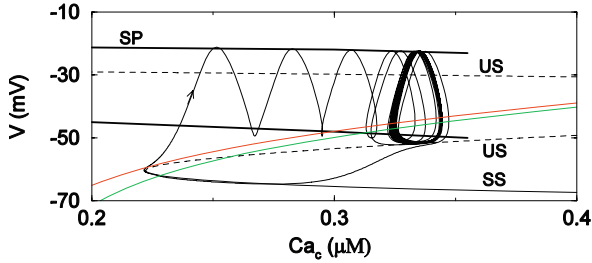


Fig. 9 Fast/slow analysis of fast bursting. The curve marked SS is a branch of stable steady states of the fast (V and n) subsystem. The curves marked US are branches of unstable steady states. The curve marked SP, and the bold curve below it represent stable periodic solutions. The burst trajectory of the full system is superimposed (thin black curve). The red and green curves are the Ca_c nullclines for $Ca_{er} = 178 \mu M$ and $Ca_{er} = 196 \mu M$, respectively. (Color figure online.)

tom thick curve) of the oscillations are shown. The bursting trajectory (thin black curve) is superimposed on the slow manifold, so that the Ca_c - V plane is treated as a phase plane of the full system.

The red and green curves in Fig. 9 are the Ca_c nullclines for two different values of Ca_{er} . The nullcline is the set of points for which the time derivative of Ca_c is zero. From Eq. (12), this yields the equation

$$Ca_c = \frac{J_{in} - k_{2b} + p_{leak}Ca_{er} + k_{pmca}Ca_{bas}}{k_{pmca} + k_3 + p_{leak}}, \tag{34}$$

which is just Eq. (19), with the addition of the Ca_{bas} term. Clearly, Ca_{er} enters into the nullcline equation, and the effect of increasing Ca_{er} is to shift the nullcline to the right in the Ca_c - V plane. Since Ca_{er} varies from 178 μM to 196 μM during bursting (Fig. 8C), we plot the Ca_c nullcline for these two values ($Ca_{er} = 178 \mu M$ for the red curve; $Ca_{er} = 196 \mu M$ for the green curve).

When the phase point is above the Ca_c nullcline, as during the active or spiking phase of bursting, it moves rightward along the periodic branch since the Ca_c derivative is positive. At $Ca_c \approx 0.33 \mu M$ the trajectory stalls and would remain in the spiking state, except that Ca_{er} slowly increases and moves the Ca_c nullcline to the right. This allows the trajectory to move slowly rightward and eventually escape the periodic branch, as it approaches a homoclinic bifurcation that terminates the branch. During the silent phase the trajectory moves leftward since it is below the Ca_c nullcline, but it again stalls near the knee at the intersection of the SS branch and the nullcline. The trajectory would remain in the silent state, except that Ca_{er} slowly declines and moves the Ca_c nullcline leftward. Eventually the nullcline moves past the knee and the trajectory escapes the steady state branch, starting a new burst. This is an example of “phantom bursting,” where the bursting is produced by the interaction of two slow variables with very different time constants (Bertram et al., 2000).

Since k_{2b} is in the Ca_c nullcline equation (Eq. (34)), inhibition of SERCA2b pumps will cause a rightward shift of the nullcline. (Note that k_{2b} does not appear in the fast subsystem, so that the slow manifold is unchanged by changes in k_{2b} .) The inhibition will also result in a decline in Ca_{er} , which will have the opposite effect on the nullcline.

After some time has elapsed, Ca_{er} will have adjusted to a level such that the nullcline will be identical to what it was before SERCA inhibition. That is, with $k_{2b} = 0$ and after transients have ended, the ER Ca^{2+} concentration oscillates between $Ca_{er} = 129 \mu\text{M}$ and $Ca_{er} = 147 \mu\text{M}$, rather than its original range of 178–196 μM . At $Ca_{er} = 129 \mu\text{M}$ the Ca_c nullcline is identical to the red nullcline in Fig. 9; at $Ca_{er} = 147 \mu\text{M}$ the nullcline is identical to the green nullcline. Thus, just as in the case of the voltage clamp pulse train, the ER Ca^{2+} concentration adjusts to the inhibition of SERCA2b pumping so that the asymptotic cytosolic Ca^{2+} is unaffected by the inhibition.

8. SERCA3 inhibition converts fast bursting to very fast bursting

Contrary to SERCA2b inhibition, SERCA3 inhibition has a dramatic effect on fast bursting, converting it to very fast bursting (Fig. 10A). The reason for this is that setting $k_3 = 0$ deforms the Ca_c nullcline, which is not unexpected, since k_3 is present in the C_∞ function obtained for a periodic pulse train (Eq. (33)). The accompanying reduction in Ca_{er} does not compensate for this deformation. With SERCA2b as the only active Ca^{2+} pump for the ER, the ER Ca^{2+} concentration does not fluctuate with the cytosolic Ca^{2+} concentration. Instead, it stays at a constant value of $Ca_{er} \approx 50 \mu\text{M}$. Fig. 10B shows the Ca^{2+} nullcline with $k_3 = 0$ and $Ca_{er} = 50 \mu\text{M}$ (blue curve), superimposed on the slow manifold (which is unaffected by k_3). Unlike before (red curve), the shape and location of the nullcline is such that the trajectory does not stall in either the silent or active phase. Instead, the trajectory moves smoothly between silent to active phases, as is typical for square wave or type I bursting (Bertram et al., 1995a; Rinzel, 1985). In this case, the burst period is determined by the time constant for Ca_c , which is much smaller than the time constant for Ca_{er} that largely determines the burst

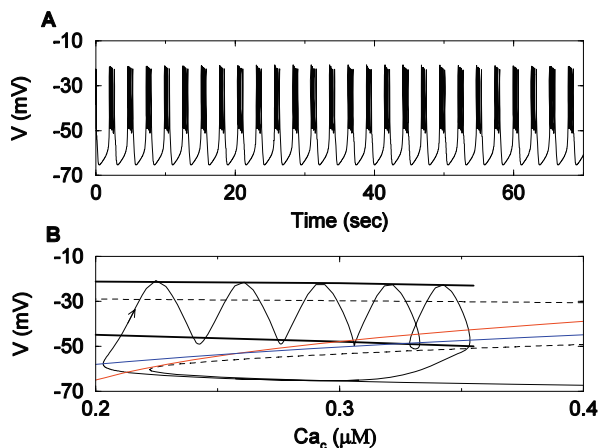


Fig. 10 (A) Very fast bursting that occurs with SERCA3 inhibition ($k_3 = 0$). (B) Fast/slow analysis of the bursting. The red nullcline is from Fig. 9 ($k_3 = 0.1$, $Ca_{er} = 178 \mu\text{M}$); the blue nullcline corresponds to SERCA3 inhibition ($k_3 = 0$, $Ca_{er} = 50 \mu\text{M}$). The burst trajectory (thin black curve) moves smoothly between the lower stationary branch and the upper periodic branch, typical of type I bursting. (Color figure online.)

period in Fig. 9. Therefore, the bursting produced by SERCA3 inhibition is very fast. Because k_{2b} has no long-term effect on the Ca_c nullcline, as was the case in Eq. (33), upregulation of SERCA2b cannot compensate for inhibition of SERCA3.

9. Store operated current (SOC) converts very fast bursting to continuous spiking

If SOC, which is activated by depletion of Ca^{2+} in the ER, is present in the cell, then inhibition of SERCA2b or SERCA3 may activate the current. We consider the case of SERCA3 inhibition, but now with $g_{\text{SOC}} = 10$ pS. Rather than the fast bursting that was produced with SERCA3 inhibition in the absence of SOC in Fig. 10, a continuous spiking pattern is now produced (Fig. 11A). This can be understood in terms of the fast/slow analysis (Fig. 11B). With SOC present, the ER Ca^{2+} concentration now affects the fast subsystem (through I_{SOC} in Eq. (7)), and, therefore, the slow manifold. When SERCA3 is inhibited and Ca_{er} declines below the threshold for activation of SOC ($70 \mu\text{M}$), the slow manifold is shifted to the right. This is because I_{SOC} is a depolarizing current with voltage-independent conductance. With this rightward shift, the Ca_c nullcline crosses deep within the periodic branch. This results in continuous spiking, rather than bursting. A more precise description can be made that utilizes the average voltage curve (thick dot-dashed curve in Fig. 11B). Each point on this curve is the average value of V during one period of the spiking oscillation. The location of the intersection of this curve with the Ca_c nullcline determines approximately where the trajectory will lie during the spiking oscillation. If the intersection is close to the homoclinic bifurcation that terminates the periodic branch, then the phase point will escape the periodic branch and bursting will occur. In Fig. 11, however, the intersection is far from the homoclinic bifurcation, so the phase point is trapped on the periodic spiking branch.

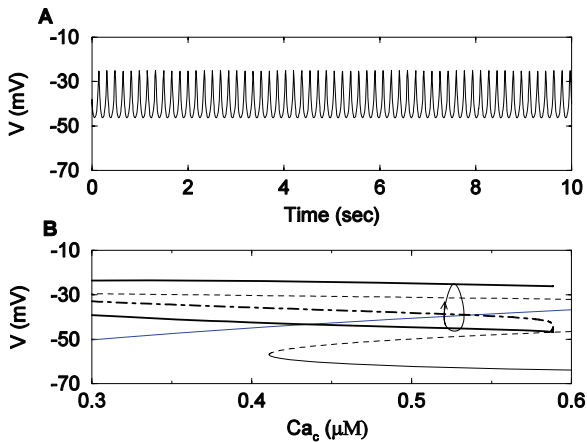


Fig. 11 (A) Continuous spiking due to SERCA3 inhibition ($k_3 = 0$) when SOC is present in the model cell ($g_{\text{SOC}} = 10$ pS). The ER Ca^{2+} concentration falls to approximately $50 \mu\text{M}$ in response to the inhibition, which is below the threshold ($70 \mu\text{M}$) for activation of SOC. (B) The depolarizing I_{SOC} translates the slow manifold to the right, so that the Ca_c nullcline (blue) and average voltage curve (thick dot-dashed) intersect deep within the periodic branch. As a result, continuous spiking is produced. (Color figure online.)

10. Discussion

We have shown that differences in the Ca^{2+} affinity of the two isoforms of the SERCA pump present in pancreatic β -cells lead to qualitative differences in their effect on cytosolic Ca^{2+} dynamics. Inhibition of SERCA2b pumps is completely compensated by a lowering of the ER Ca^{2+} concentration, so that after an initial transient, the dynamics of the cytosolic Ca^{2+} are identical to the dynamics before inhibition. However, if Ca_{er} falls so low that it activates store-operated current, then this depolarizing current will speed up oscillations. Inhibition of SERCA3 pumps has a dramatic effect on cytosolic Ca^{2+} dynamics, tending to speed up bursting oscillations even in the absence of SOC. In our analysis, the key difference between the two isoforms is that one has a relatively low Ca^{2+} affinity (SERCA3), while the other has a high affinity and is assumed to be saturated at physiological Ca^{2+} levels (SERCA2b).

The motivation for this work was to understand recent data showing that islets from SERCA3 knockout mice do not exhibit compound Ca^{2+} oscillations, as are commonly observed in islets from control mice (Beauvois et al., 2006). We demonstrated in Figs. 3–4 that this is reproduced by our Dual Oscillator Model for the β -cell (Bertram et al., 2007b), which contains compartments for electrical activity, calcium handling, glycolysis, and mitochondrial respiration. However, to explain the behavior it is convenient to focus on the components responsible for the fast bursting that occurs in episodes during compound bursting, since the slow outer oscillations of the compound burst (which are driven by the metabolic compartments of the model) are not significantly effected by SERCA3 inhibition. Using this approach, we found that SERCA3 inhibition converts fast bursting to very fast bursting, or continuous spiking if SOC is present. This explains why compound bursting is converted to slow bursting (Figs. 3–4): the slow outer oscillations persist, but the fast bursting inner oscillations are converted to continuous spiking or very fast bursting.

Although there is, to our knowledge, no parallel data on SERCA2b knockout mice, we wished to see how SERCA2b inhibition would affect the Ca^{2+} dynamics of the model β -cell. Using periodic voltage pulses we proved that the ER Ca^{2+} concentration compensates for SERCA2b inhibition, so that there is no long-term effect on the cytosolic Ca^{2+} response to the voltage pulses. Similarly, there is no long-term effect on fast bursting following SERCA2b inhibition, unless the ER Ca^{2+} concentration falls to a level low enough to activate SOC. This explains the lack of effect on compound bursting shown in Fig. 5. We predict then that any effect of SERCA2b inhibition on the long-term pattern of cytosolic Ca^{2+} oscillations would be due to activation of SOC; without SOC there would be no effect.

We made several assumptions in our analysis. First, we assumed that the SERCA2b pumps are saturated at physiological levels of Ca^{2+} , motivated by findings from two studies that the Ca^{2+} affinity for these pumps is high (Verboomen et al., Lytton et al.). These studies were done by expressing SERCA2b in COS 1 cells, and the value of the $K_{1/2}$ varied significantly between the two studies, so the value of the $K_{1/2}$ is not known in β -cells. We used saturated SERCA2b pumps, rather than a Hill function with a small Hill coefficient, so that analytical expressions could be obtained for the Ca^{2+} subsystem (Sections 5 and 6). A second assumption is that the SERCA3 pumps depend linearly on Ca^{2+} . This is motivated by the finding that the Ca^{2+} affinity of these pumps is low (Lytton), so that the $K_{1/2}$ is large. A linear expression was used, rather than a Hill function with large Hill

coefficient, to again facilitate the analysis. Several SERCA pump models have been developed that are more mechanistically accurate than the simple linear model (Sneyd and others), and use of these more sophisticated models is recommended when studying ER-induced Ca^{2+} oscillations (Sneyd). However, in our case where the oscillations are driven by Ca^{2+} flux through the plasma membrane, a linear expression should suffice. Indeed, we have found that the key results (Figs. 3–5) can be reproduced when a function of the form (Sneyd et al., 2003):

$$J_{\text{SERCA3}} = \left(\frac{V_{\text{SERCA3}} \text{Ca}_c}{K_{\text{SERCA3}} + \text{Ca}_c} \right) \left(\frac{1}{\text{Ca}_{er}} \right) \quad (35)$$

is used (not shown). The third assumption that we make is that the fast bursting that occurs during an episode of compound bursting is driven by the slow variables Ca_c and Ca_{er} . With different parameter values, the model can be adjusted so that bursting is driven instead by Ca_c and cytosolic ATP (Biophan paper). In this case, inhibiting SERCA3 in the absence of SOC current does not convert compound bursting to slow bursting, as in Fig. 4.

Compound and slow Ca^{2+} oscillations in pancreatic islets are likely to have physiological relevance, since the period of these oscillations is similar to the period of blood insulin oscillations (Bergsten and Hellman, 1993; Nunemaker et al., 2005; Pørksen et al., 1995). It is not known if compound Ca^{2+} oscillations are in any way physiologically preferential to slow oscillations, but we have suggested that the two oscillatory components of compound bursts provide the means for transducing changes in blood glucose concentration to changes in insulin secretion. (There is also an amplifying pathway that is independent of Ca^{2+} Henquin, 2000.) According to this “Metronome Hypothesis,” the plateau fraction (fraction of active phase duration to total burst period) of the inner bursts increases when the glucose concentration increases, while the slow outer oscillations are relatively unaffected (Bertram et al., 2007b). As a result, more insulin is secreted during each episode of fast bursts, but the frequency at which episodes occur is largely unchanged. Thus, the amplitude of the insulin oscillations increases with an increase in glucose concentration, while the period remains relatively unchanged. This behavior is what is typically observed (Bergsten and Hellman, 1993). In light of this hypothesis, one physiological effect of SERCA3 inhibition or knockout would be to short-circuit this mechanism for a proper secretory response to changes in the glucose concentration.

Acknowledgement

This work was partially supported by NSF grant DMS-0613179 to RB.

References

- Arredouani, A., Guiot, Y., Jonas, J.-C., Liu, L.H., Nenquin, M., Pertusa, J.A., Rahier, J., Rolland, J.-F., Shull, G.E., Stevens, M., Wuytack, F., Henquin, J.C., Gilon, P., 2002a. SERCA3 ablation does not impair insulin secretion but suggests distinct roles of different sarcoendoplasmic reticulum Ca^{2+} pumps for Ca^{2+} homeostasis in pancreatic β -cells. *Diabetes* 51, 3245–3253.
- Arredouani, A., Henquin, J.-C., Gilon, P., 2002b. Contribution of the endoplasmic reticulum to the glucose-induced $[\text{Ca}^{2+}]_c$ response in mouse pancreatic islets. *Am. J. Physiol.* 282, E982–E991.

- Ashcroft, F.M., Harrison, D.E., Ashcroft, S.J.H., 1984. Glucose induces closure of single potassium channels in isolated rat pancreatic β -cells. *Nature* 312, 446–448.
- Beauvois, M.C., Merezak, C., Jonas, J.-C., Ravier, M.A., Henquin, J.-C., 2006. Glucose-induced mixed $[Ca^{2+}]_c$ oscillations in mouse β -cells are controlled by the membrane potential and the SERCA3 Ca^{2+} -ATPase of the endoplasmic reticulum. *Am. J. Physiol.* 290, C1503–C1511.
- Bergsten, P., 1995. Slow and fast oscillations of cytoplasmic Ca^{2+} in pancreatic islets correspond to pulsatile insulin release. *Am. J. Physiol.* 268, E282–E287.
- Bergsten, P., Hellman, B., 1993. Glucose-induced amplitude regulation of pulsatile insulin secretion from individual pancreatic islets. *Diabetes* 42, 670–674.
- Bergsten, P., Grapengiesser, E., Gylfe, E., Tengholm, A., Hellman, B., 1994. Synchronous oscillations of cytoplasmic Ca^{2+} and insulin release in glucose-stimulated pancreatic islets. *J. Biol. Chem.* 269, 8749–8753.
- Bertram, R., Sherman, A., 2004a. A calcium-based phantom bursting model for pancreatic islets. *Bull. Math. Biol.* 66, 1313–1344.
- Bertram, R., Sherman, A., 2004b. Filtering of calcium transients by the endoplasmic reticulum in pancreatic β -cells. *Biophys. J.* 87, 3775–3785.
- Bertram, R., Butte, M., Kiemel, T., Sherman, A., 1995a. Topological and phenomenological classification of bursting oscillations. *Bull. Math. Biol.* 57, 413–439.
- Bertram, R., Smolen, P., Sherman, A., Mears, D., Atwater, I., Martin, F., Soria, B., 1995b. A role for calcium release-activated current (CRAC) in cholinergic modulation of electrical activity in pancreatic β -cells. *Biophys. J.* 68, 2323–2332.
- Bertram, R., Previde, J., Sherman, A., Kinard, T.A., Satin, L.S., 2000. The phantom burster model for pancreatic β -cells. *Biophys. J.* 79, 2880–2892.
- Bertram, R., Satin, L., Zhang, M., Smolen, P., Sherman, A., 2004. Calcium and glycolysis mediate multiple bursting modes in pancreatic islets. *Biophys. J.* 87, 3074–3087.
- Bertram, R., Satin, L.S., Pedersen, M.G., Luciani, D.S., Sherman, A., 2007a. Interaction of glycolysis and mitochondrial respiration in metabolic oscillations of pancreatic islets. *Biophys. J.* 92, 1544–1555.
- Bertram, R., Sherman, A., Satin, L.S., 2007b. Metabolic and electrical oscillations: Partners in controlling pulsatile insulin secretion. *Am. J. Physiol.* 293, E890–E900.
- Cook, D.L., 1983. Isolated islets of Langerhans have slow oscillations of electrical activity. *Metabolism* 32, 681–685.
- Cook, D., Porte, D.J., Crill, W.E., 1981. Voltage dependence of rhythmic plateau potentials of pancreatic islet cells. *Am. J. Physiol.* 240, E290–E296.
- Dahlgren, G.M., Kauri, L.M., Kennedy, R.T., 2005. Substrate effects on oscillations in metabolism, calcium and secretion in single mouse islets of Langerhans. *Biochim. Biophys. Acta* 1724, 23–36.
- Ermentrout, G.B., 2002. *Simulating, Analyzing, and Animating Dynamical Systems: A Guide to XPPAUT for Researchers and Students*. SIAM, Philadelphia.
- Gilon, P., Arredouani, A., Gailly, P., Gromada, J., Henquin, J.-C., 1999. Uptake and release of Ca^{2+} by the endoplasmic reticulum contribute to the oscillations of the cytosolic Ca^{2+} concentration triggered by Ca^{2+} influx in the electrically excitable pancreatic β -cell. *J. Biol. Chem.* 274, 20197–20205.
- Henquin, J.C., 1988. ATP-sensitive K^+ channels may control glucose-induced electrical activity in pancreatic β -cells. *Biochem. Biophys. Res. Commun.* 156, 769–775.
- Henquin, J.C., 2000. Triggering and amplifying pathways of regulation of insulin secretion by glucose. *Diabetes* 49, 1751–1760.
- Henquin, J.C., Meissner, H.P., Schmeer, W., 1982. Cyclic variations of glucose-induced electrical activity in pancreatic B cells. *Pflügers Archiv.* 393, 322–327.
- Liu, Y.-J., Grapengiesser, E., Gylfe, E., Hellman, B., 1995. Glucose induces oscillations of cytoplasmic Ca^{2+} , Sr^{2+} and Ba^{2+} in pancreatic β -cells without participation of the thapsigargin-sensitive store. *Cell. Calcium.* 18, 165–173.
- Liu, Y.-J., Tengholm, A., Grapengiesser, E., Hellman, B., Gylfe, E., 1998. Origin of slow and fast oscillations of Ca^{2+} in mouse pancreatic islets. *J. Physiol.* 508, 471–481.
- Mears, D., Zimlik, C.L., 2004. Muscarinic agonists activate Ca^{2+} store-operated and independent ionic currents in insulin-secreting HIT-T15 cells and mouse pancreatic β -cells. *J. Membr. Biol.* 197, 59–70.
- Miura, Y., Henquin, J.C., Gilon, P., 1997. Emptying of intracellular Ca^{2+} stores stimulates Ca^{2+} entry in mouse pancreatic β -cells by both direct and indirect mechanisms. *J. Physiol.* 503, 387–398.
- Nunemaker, C.S., Zhang, M., Wasserman, D.H., McGuinness, O.P., Powers, A.C., Bertram, R., Sherman, A., Satin, L.S., 2005. Individual mice can be distinguished by the period of their islet calcium oscillations: Is there an intrinsic islet period that is imprinted in vivo? *Diabetes* 54, 3517–3522.

- Pørksen, N., Munn, S., Steers, J., Vore, S., Veldhuis, J., Butler, P., 1995. Pulsatile insulin secretion accounts for 70% of total insulin secretion during fasting. *Am. J. Physiol.* 269, E478–E488.
- Rinzel, J., 1985. Bursting oscillations in an excitable membrane model. In: Sleeman, B.D., Jarvis, R.J. (Eds.), *Ordinary and Partial Differential Equations. Lecture Notes in Mathematics*, pp. 304–316. Springer, New York.
- Roe, M.W., Worley III, J.F., Qian, F., Tamarina, N., Mittal, A.A., Dralyuk, F., Blair, N.T., Mertz, R.J., Philipson, L.H., Dukes, I.D., 1998. Characterization of a Ca^{2+} release-activated nonselective cation current regulating membrane potential and $[\text{Ca}^{2+}]_i$ oscillations in transgenetically derived β -cells. *J. Biol. Chem.* 273, 10402–10410.
- Santos, R.M., Rosario, L.M., Nadal, A., Garcia-Sancho, J., Soria, B., Valdeolmillos, M., 1991. Widespread synchronous $[\text{Ca}^{2+}]_i$ oscillations due to bursting electrical activity in single pancreatic islets. *Pflügers Archiv.* 418, 417–422.
- Smolen, P., 1995. A model for glycolytic oscillations based on skeletal muscle phosphofructokinase kinetics. *J. Theor. Biol.* 174, 137–148.
- Sneyd, J., Tsaneva-Atanasova, K., Bruce, J.I.E., Straub, S.V., Giovannucci, D.R., Yule, D.I., 2003. A model of calcium waves in pancreatic and parotid acinar cells. *Biophys. J.* 85, 1392–1405.
- Tornheim, K., 1979. Oscillations of the glycolytic pathway and the purine nucleotide cycle. *J. Theor. Biol.* 79, 491–541.
- Tornheim, K., 1997. Are metabolic oscillations responsible for normal oscillatory insulin secretion? *Diabetes* 46, 1375–1380.
- Tornheim, K., Lowenstein, J.M., 1974. The purine nucleotide cycle: IV. Interactions with oscillations of the glycolytic pathway in muscle extracts. *J. Biol. Chem.* 249, 3241–3247.
- Tornheim, K., Lowenstein, J.M., 1975. The purine nucleotide cycle: Control of phosphofructokinase and glycolytic oscillations in muscle extracts. *J. Biol. Chem.* 250, 6304–6314.
- Tornheim, K., Lowenstein, J.M., 1976. Control of phosphofructokinase from rat skeletal muscle: effects of fructose diphosphate, AMP, ATP, and citrate. *J. Biol. Chem.* 251, 7322–7328.
- Váradi, A., Molnár, E., Östenson, C.G., Ashcroft, S.J.H., 1996. Isoforms of endoplasmic reticulum Ca^{2+} -ATPase are differentially expressed in normal and diabetic islets of Langerhans. *Biochem. J.* 319, 521–527.
- Yaney, G.C., Schultz, V., Cunningham, B.A., Dunaway, G.A., Corkey, B.E., Tornheim, K., 1995. Phosphofructokinase isozymes in pancreatic islets and clonal β -cells (INS-1). *Diabetes* 44, 1285–1289.
- Zhang, M., Goforth, P., Sherman, A., Bertram, R., Satin, L., 2003. The Ca^{2+} dynamics of isolated mouse β -cells and islets: Implications for mathematical models. *Biophys. J.* 84, 2852–2870.